CP/MAS ^{13}C NMR Analyses of the Chain Conformation and Hydrogen Bonding for Frozen Poly(vinyl alcohol) Solutions

Kenji Masuda and Fumitaka Horii*

Institute for Chemical Research, Kyoto University, Uji, Kyoto 611-0011, Japan

Received January 29, 1998; Revised Manuscript Received May 13, 1998

ABSTRACT: CP/MAS ^{13}C NMR analyses have been made for different frozen solutions of poly(vinyl alcohol) (PVA) samples with different tacticities to obtain further information about the intramolecular hydrogen bonding of PVA. Aqueous or deuterated dimethyl sulfoxide (DMSO-d_6) solutions (3 wt %) have been frozen in a rotating MAS rotor by cooling to −50 °C. The CH resonance lines of the frozen PVA solutions split in different ways, significantly depending on the tacticities and the solvents. These CH resonance lines can be well resolved into six to eight constituent lines by the least-squares method, whose lines have different chemical shifts evaluated by assuming the downfield shifts due to the intramolecular hydrogen bonding and the upfield shifts induced by the *γ-gauche* effect. Furthermore, the relative intensities of the lines thus resolved are successfully interpreted for the frozen atactic PVA solutions by the statistical treatment assuming the statistical formation of the intramolecular hydrogen bonds and the random distribution of the trans and gauche conformations along the PVA chains. The probabilities of the trans conformation and the intramolecular hydrogen bond are also determined through this analysis for atactic PVA samples. In contrast, such calculations based on Bernoullian statistics cannot be applied to the cases of the frozen isotactic PVA solutions, suggesting that certain specific conformations are preferably formed for the isotactic PVA samples.

Introduction

Conventional almost atactic poly(vinyl alcohol) (PVA) is widely used as films, hydrogels, and fibers for its high heat-resistance, hydrophilic properties, adhesive properties, and alkali resistance.[1,2] The main chain has a planar zigzag conformation in the crystalline region as in the case of polyethylene, and the tensile modulus along the molecular chain axis is significantly higher than that of polyethylene. It is, therefore, expected that higher modulus and higher tenacity films or fibers will be produced from PVA. However, they are not still realized probably because of the difficulty in controlling the intramolecular and intermolecular hydrogen bonds during the real processing.

It is well-known that the resonance line for the CH carbons, which are bonded to OH groups, splits into three lines (lines I−III) in the CP/MAS ^{13}C NMR spectra of solid PVA. Such a split, at least in the crystalline component, was simply attributed to the formation of two, one, and no intramolecular hydrogen bond(s) in the triad sequences.[3−5] In contrast, another interpretation in terms of the substitution effects of OH groups was proposed from the experimental and theoretical sides.[6,7] We have recently confirmed the validity of the previous assignment based on the formation of intramolecular hydrogen bonding by clarifying that the relative intensities of lines I−III significantly depend on the water content, draw ratio, casting solvents, and annealing temperatures even for PVA samples with the same tacticities.[4,5,8−11] Moreover, the probability for the formation of the intramolecular hydrogen bond in the meso sequence was determined for different PVA samples by the simple statistical treatment[5,8,9] based on the crystal structure[12,13] of PVA. A recent preliminary report of the CP/MAS ^{13}C NMR for frozen PVA solutions also supports that the characteristic splitting of the CH resonance line is due to the formation of the intramolecular hydrogen bonding.[14]

Table 1. Degrees of Polymerization (DP) and Tacticities for Different PVA Samples

		triad tacticity			diad tacticity[a]	
sample	DP	*mm*	*mr*	*rr*	*m*	*r*
A-PVA	1700	0.23	0.50	0.27	0.48	0.52
LI-PVA	*b*	0.50	0.39	0.11	0.70	0.30
MI-PVA	1130	0.66	0.28	0.06	0.81	0.19
HI-PVA	9100	0.79	0.19	0.02	0.88	0.12

[a] Calculated by the least-squares method assuming Bernoullian statistics. [b] Not measured.

In this paper, we have measured CP/MAS ^{13}C NMR spectra of the frozen deuterated dimethyl sulfoxide (DMSO-d_6) and aqueous solutions of PVA samples with different isotacticities. The CH lines thus obtained, which split in different ways depending on the tacticities and solvents, have been analyzed by the statistical treatment considering the random distribution of trans and gauche conformations along PVA chains as well as the statistical formation of the intramolecular hydrogen bonds between the appropriate adjacent OH groups. This study will be the first statistical NMR analysis of the hydrogen bonding and conformation for synthetic polymers in the frozen solution state. It is also found that such frozen-solution-state CP/MAS ^{13}C NMR spectroscopy is another widely applicable NMR method to characterize some important properties in solutions that may be averaged out in real solutions by rapid molecular motions.

Experimental Section

Samples. Almost atactic PVA (A-PVA) and different isotactic PVAs with different levels (LI-PVA, MI-PVA, HI-PVA[15]), which were provided by Kuraray Co., were used after the purification through complete saponification. Table 1 shows viscosity-average degrees of polymerization (DP) and triad and diad tacticities determined at 50 °C in deuterated dimethyl sulfoxide (DMSO-d_6) by gated scalar decoupling ^{13}C NMR

S0024-9297(98)00126-0 CCC: $15.00
Published on Web 08/05/1998

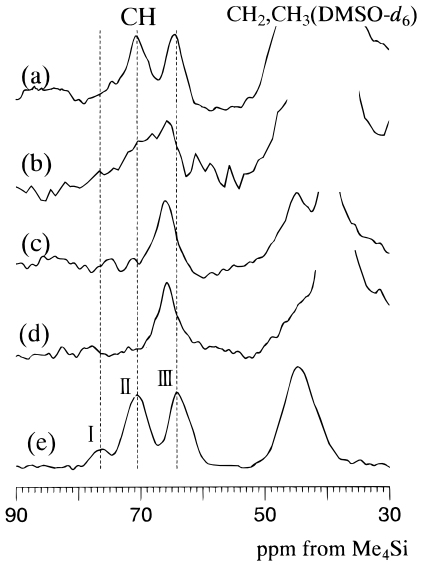

Figure 1. CP/MAS ^{13}C NMR spectra of frozen DMSO-d_6 solutions of PVA samples with different tacticities, measured at −50 °C: (a) A-PVA; (b) LI-PVA; (c) MI-PVA; (d) HI-PVA; (e) crystalline component of A-PVA films prepared from DMSO solution.

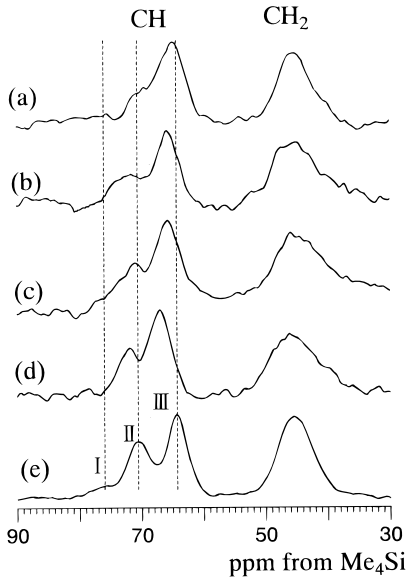

Figure 2. CP/MAS ^{13}C NMR spectra of frozen aqueous solutions of PVA samples with different tacticities, measured at −50 °C: (a) A-PVA; (b) LI-PVA; (c) MI-PVA; (d) HI-PVA; (e) crystalline component of A-PVA films prepared from aqueous solution.

spectroscopy. Each PVA was dissolved in 3 wt % deionized water or DMSO-d_6 at 120 °C for A-PVA and HI-PVA and at 60 °C for LI-PVA and MI-PVA in a glass tube sealed under an atmosphere of argon. Each solution thus obtained was packed into a cylindrical MAS rotor with an O-ring seal[4,16] and frozen in the rotating state at a rate of about 1 kHz in a CP/MAS probe by decreasing the temperature down to −50 °C. Almost the same clear aqueous or DMSO-d_6 solutions were obtained at room temperature after the NMR measurements, indicating no apparent formation of gels in these systems.

CP/MAS ^{13}C NMR measurements. CP/MAS ^{13}C NMR spectra of the frozen PVA solutions were measured at −50 °C on a JEOL JNM-GSX200 spectrometer operating at a static magnetic field of 4.7 T. ^{1}H and ^{13}C radio frequency field strengths $\gamma B_1/2\pi$ were 69.4 kHz as estimated from the 90° pulse width. The contact time for the CP process was set to 1 ms, and the delay time after the acquisition of a free induction decay was 5 s throughout this work. ^{13}C chemical shifts relative to tetramethylsilane (Me_4Si) were determined by using the CH_3 line at 17.36 ppm of hexamethylbenzene crystals as an external reference. The CPT1 pulse sequence[17] was used for T_{1C} measurements.

Results and Discussion

CP/MAS ^{13}C NMR Spectra and ^{13}C Spin−Lattice Relaxation Times. We have already confirmed that the CH resonance lines in CP/MAS ^{13}C NMR spectra of frozen PVA solutions are not significantly changed in appearance by the concentration ranging from 3 to 10 wt %.[14] Therefore, we analyze only 3 wt % PVA solutions in this study.

Figure 1 shows CP/MAS ^{13}C NMR spectra of frozen DMSO-d_6 solutions of PVA samples with different tacticities, which were measured at −50 °C. In this figure, for reference, is also shown the CP/MAS ^{13}C NMR spectrum of the crystalline component for A-PVA films prepared from 10 wt % DMSO solution, which was selectively measured at room temperature by the CPT1 pulse sequence.[4,17] Here, the contributions from the materials used for the MAS rotor and the probe were removed by subtracting the spectrum obtained by the blank measurement from the corresponding spectra. The broken lines indicate ^{13}C chemical shifts of lines I−III in the crystalline state. The CH resonance line of the frozen A-PVA/DMSO-d_6 solution clearly splits into two lines, and these two lines have the same chemical shifts as for lines I and III. In the frozen LI-PVA solution, however, the CH resonance line does not split clearly, possibly due to the upfield shift of the downfield line and the downfield shift of the upfield line. When the *mm* fraction is further increased, only a single line appears, as show in Figure 1c,d. Moreover, the chemical shift of the single line is in disagreement with that of line II or III.

Figure 2 shows CP/MAS ^{13}C NMR spectra of frozen aqueous solutions of PVA samples with different tacticities. For reference, the CP/MAS ^{13}C NMR spectrum of the crystalline component for A-PVA films prepared from 10 wt % aqueous solution is also shown in this figure. In the frozen A-PVA aqueous solution, two lines appear at the chemical shifts corresponding to lines II and III, but the relative intensity significantly differs from that of the crystalline component. Moreover, these lines remarkably shift downfield with increasing *mm* fraction.

As shown in Figures 1 and 2, the splitting, chemical shifts, and relative intensities of the CH lines greatly depend on the tacticities and solvents. These results will be interpreted in terms of the downfield shift due to the formation of the intramolecular hydrogen bonds as well as the upfield shifts induced by the so-called γ-gauche effect,[18] as described in detail in the following section.

To confirm that the respective frozen PVA solutions are composed of single components, ^{13}C spin−lattice relaxation times (T_{1C}) were measured by the CPT1 pulse sequence.[17] As a result, the T_{1C} decay curve for each CH line was found to be described as a single exponential, the T_{1C} value ranging from 10 to 30 s. This fact indicates that each PVA chain may be well dispersed in the respective frozen media without any phase separation that produces phases with different PVA concentrations. Moreover, the mobility of the structural units of PVA should be restricted at the same level as

for the noncrystalline component in A-PVA films below T_g, because the T_{1C} values described above are of the same order as the values for the noncrystalline component measured at room temperature.[4,5] In contrast, it was found that residual CH_3 groups of DMSO-d_6 consist of two components with T_{1C} values of about 0.1 and 1.3 s. Since the mole fractions of these components were estimated to be about 0.5, it seems difficult to simply assign them to CH_3 groups of DMSO molecules bound and nonbound to OH groups. There may exist two phases, the pure DMSO phase and the PVA/DMSO phase. In fact, a rather broad endothermic peak was observed at about 17 °C by differential scanning calorimetry, when the 3.0% frozen PVA/DMSO-d_6 solution was heated from −50 °C at a rate of 10 °C min^{-1}. Although more detailed characterization of the two components should be made in near future, each PVA molecule is assumed to be surrounded by equivalent DMSO molecules from the point of view of molecular mobility associated with T_{1C} values.

Effects of the Gauche Conformation and the Intramolecular Hydrogen Bonding on ^{13}C Chemical Shifts. To interpret the differences in splitting, chemical shift, and relative intensity, observed in Figures 1 and 2, we have performed somewhat simple calculations considering the upfield shift by the γ-gauche effect[18,19] and the downfield shift by the formation of the intramolecular hydrogen bond. The effect of intermolecular hydrogen bonding is ignored in analogy with the case of the crystalline component of PVA. According to the crystal structure of PVA,[12,13] the oxygen−oxygen distance is longer than 0.27 nm for the intermolecular hydrogen bonds while it is as short as 0.252 nm for the intramolecular hydrogen bonds. The previous study[20] clarified by using hydroxybenzaldehyde crystals that there is almost no effect of hydrogen bonding on ^{13}C chemical shifts when the oxygen−oxygen distance is longer than 0.27 nm. Therefore, the ignorance of the effect of intermolecular hydrogen bonding may be acceptable. We also neglect the effect of the solvation as the first approximation, because this effect seems comparatively minor, like the effect of intermolecular hydrogen bonding, and the estimation of this effect has not yet been established in the frozen state.

In the frozen PVA solutions, the gauche conformation should exist and then the downfield shift will be induced for the CH line as a result of the γ-gauche effect. Here, the γ-gauche effect is the conformational effect on the chemical shift of the C_0 carbon in the $C_0-C_\alpha-C_\beta-X_\gamma$ sequence; the gauche conformation in the $C_\alpha-C_\beta$ bond induces a 5−8 ppm upfield shift for the C_0 carbon compared to the case of the trans conformation. In this work, the γ-gauche effects due to the CH_2 carbon and the OH oxygen are assumed as follows according to reported results:[18] $\gamma_{C-C} = -5.9$ ppm and $\gamma_{C-O} = -7.2$ ppm. Furthermore, the downfield shift ($\Delta\delta_{intra}$) induced by the formation of the single intramolecular hydrogen bond is assumed to be +5.9 ppm on the basis of the results for the crystalline components of different PVA samples.[4,5,8−11]

Figure 3 shows two examples to give different chemical shifts for the central CH carbon in the *mm* sequence due to the different conformations and the formation of the intramolecular hydrogen bond. Here, the conformations of two successive bonds at both sides of the central CH carbon are described as *tt*•*tt* (a) and g^-t•*tt* (b). Broken lines indicate the formation of the intramolecular hydrogen bond. In the *tt*•*tt* conformation, there are three possible states for the intramolecular hydrogen bonding; two, one, or no intramolecular hydrogen bond(s). In these cases, there is also the γ-gauche effect induced by the two OH groups at both neighboring sides. Therefore, the following three chemical shifts are possible for the central CH carbon in the *tt*•*tt* conformation for the *mm* sequence:

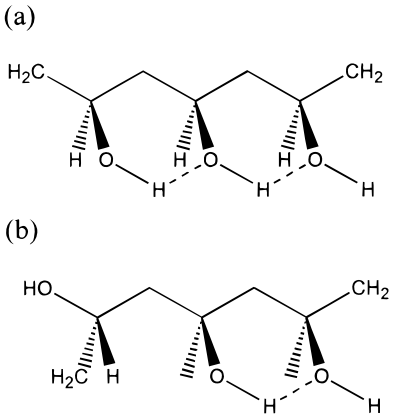

Figure 3. Schematic diagrams for the conformation and the intramolecular hydrogen bonding in the *mm* sequence: (a) *tt*•*tt*; (b) g^-t•*tt*.

$$\Delta\delta = 2\gamma_{C-O} + 2\Delta\delta_{intra} = -2.6 \text{ ppm} \quad (1)$$

$$\Delta\delta = 2\gamma_{C-O} + \Delta\delta_{intra} = -8.5 \text{ ppm} \quad (2)$$

$$\Delta\delta = 2\gamma_{C-O} = -14.4 \text{ ppm} \quad (3)$$

In the case of the g^-t•*tt* conformation, one or no intramolecular hydrogen bond can be formed, and the γ-gauche effect should be induced by the methylene carbon at the one side and by the OH oxygen at the other side, as shown in Figure 3b. As a result, the two following chemical shifts are allowed in the g^-t•*tt* conformation:

$$\Delta\delta = \gamma_{C-O} + \gamma_{C-C} + \Delta\delta_{intra} = -7.2 \text{ ppm} \quad (4)$$

$$\Delta\delta = \gamma_{C-O} + \gamma_{C-C} = -13.1 \text{ ppm} \quad (5)$$

Similar calculations have been conducted for all possible conformations in the *mm*, *mr*, and *rr* sequences. Finally, nine states with different chemical shifts are found to exist according to the differences in the intramolecular hydrogen bond and conformation. Table 2 shows these nine states as lines 1−9 in the order of increasing field together with corresponding conformations, coefficients of the respective terms for the γ-gauche effect and the formation of the intramolecular hydrogen bonding, and chemical shifts ($\Delta\delta$). In this table, symbol @ indicates either *t*, g^+, and g^- conformation.

Line Shape Analyses of the CH Resonance Lines for Frozen A-PVA Solutions. Using the nine lines with different chemical shifts listed in Table 2, line shape analyses have been conducted for the CH resonance lines of the frozen A-PVA solutions by the computer-aided least-squares method, as shown in Figure 4. Here, each line is assumed to be described as a Gausssian and the chemical shift in ppm from Me_4Si has been determined by referring line 6 shown in Table 2 to line III for the crystalline component. The

Table 2. Nine Constituent Lines, Their Conformations, Coefficients of the Respective Terms Associated with the γ-Gauche Effects and Intramolecular Hydrogen Bonding, and Total Shifts $\Delta\delta$ for the Constituent Lines

line	conformation[a]	coefficients of the respective terms γ_{C-C}	γ_{C-O}	$\Delta\delta_{intra}$	$\Delta\delta$/ppm
1	*tt*•*tt*	0	2	2	−2.6
2	*tt*•@•g^-, g^+@•*tt*	1	1	1	−7.2
3	*tt*•@•*t*, *t*@•*tt*	0	2	1	−8.5
	tt•g^-g^+, g^-g^+•*tt*	1	2	2	−8.5
4	g^+@•@•g^-	2	0	0	−11.8
5	g^+@•@•*t*, *t*@•@•g^-	1	1	0	−13.1
	g^+@•g^-•g^+, g^-@•g^-g^+	2	1	1	−13.1
6	*tt*•@•g^+, g^-@•*tt*	1	2	1	−14.4
	t@•@•*t*	0	2	0	−14.4
7	g^-@•@•g^-, g^+@•@•g^+	2	1	0	−19.0
8	g^-@•@•*t*, *t*@•@•g^+	1	2	0	−20.3
	g^-@•g^-g^+, g^-g^+•@•g^+	2	2	1	−20.3
9	g^-@•@•g^+	2	2	0	−26.2

[a] @: *t*, g^+, or g^- conformation.

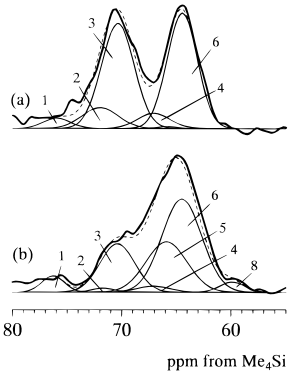

Figure 4. Line shape analyses for the CH resonance lines of different frozen A-PVA solutions: (a) DMSO-d_6; (b) H_2O. The broken line indicates the composite curve of the constituent lines shown by thin solid lines.

composite curve of the respective lines, shown by a broken line, is in good agreement with the observed resonance line indicated by a thick solid line in each frozen solution. These results indicate that the above-described assumptions for effects of the intramolecular hydrogen bonding and the γ-gauche conformation on ^{13}C chemical shifts are reasonably made. In the frozen A-PVA/DMSO-d_6 solution, lines 3 and 6 are much enhanced in intensity, while lines 3, 5, and 6 are the three main contributions in the frozen A-PVA aqueous solution. It is, therefore, found that the relative intensities of the respective lines strongly depend on solvents, reflecting the differences in contributions from the γ-gauche conformation and the intramolecular hydrogen bonding in the frozen state. To interpret the relative intensities of the CH resonance lines, simple calculations based on Bernoullian statistics have been carried out as described below.

Statistical Calculations for the Relative Intensities of the CH Lines. Numerical equations for the relative intensities of the CH resonance lines have been derived by the statistical treatment as functions of the probability f_t of the trans conformation and the probability f_a of the formation of the intramolecular hydrogen bond. Here, f_t is the probability that a given C−C bond adopts the trans conformation, while f_a is the probability that the OH group bonded to the CH carbon in question forms the intramolecular hydrogen bond with a neighboring possible OH group. Table 3 shows

Table 3. Probabilities of the Respective Constituent Lines for the *mm* Sequence[a]

line (i)	f_i^{mm}
1	$f_a^2 f_t^4$
2	$f_a^2(1-f_t)f_t^2$
3	$2f_af_t^2\{(1-f_a)f_t + 2f_af_{g^+}(1-f_t-f_{g^+})\}$
4	$f_{g^+}(1-f_t-f_{g^+})$
5	$(1-f_af_t)f_t(1-f_t) + f_a(1-f_t)f_{g^+}(1-f_t-f_{g^+})$
6	$f_t^2[(1-f_af_t)^2 + f_a\{(1-f_t) - 2f_af_{g^+}(1-f_t-f_{g^+})\}]$
7	$(1-f_t)^2 - f_a(1-f_t)f_{g^+}(1-f_t-f_{g^+}) - 2f_{g^+}^2 + 2f_{g^+}^2$
8	$\{(1-f_af_t)f_t + (1-f_t)^2f_{g^+}(1-f_t-f_{g^+})\}\{1 - 2f_af_{g^+}(1-f_t-f_{g^+})\}$
9	$f_{g^+}(1-f_t-f_{g^+})(1-f_af_{g^+})\{(1-f_a(1-f_t-f_{g^+})\}$

[a] f_{g^+}: The mole fraction of the f_{g^+} conformation.

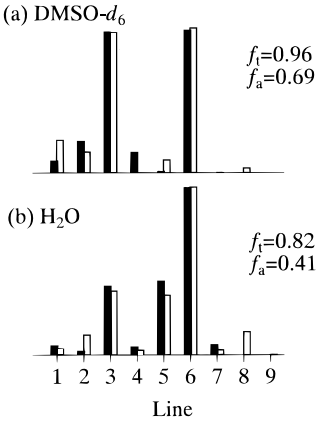

Figure 5. Histograms for observed and calculated relative intensities for the nine constituent lines in the frozen A-PVA solutions. The closed and open histograms indicate observed and calculated intensities, respectively: (a) DMSO-d_6; (b) H_2O.

the probabilities f_i^{mm} for lines $i = 1-9$ giving different chemical shifts for the *mm* sequence (see Appendix). Since similar probabilities f_i^{mr} and f_i^{rr} are obtained for the *mr* and *rr* sequences, total probabilities F_i for lines $i = 1-9$, which correspond to their relative intensities, are expressed as

$$F_i = g_{mm} f_i^{mm} + g_{mr} f_i^{mr} + g_{rr} f_i^{rr} \qquad (6)$$

Here, g_{mm}, g_{mr}, and g_{rr} are the mole fractions of the *mm*, *mr*, and *rr* sequences, respectively. Therefore, f_t and f_a values should be determined as a result of the best fit trial between observed and calculated intensities by the least-squares method.

Analyses for Different PVA Samples. Figure 5 shows the observed integrated intensities obtained for the frozen A-PVA solutions by the line shape analysis shown in Figure 4 and the calculated intensities given by eq 6 as histograms for the respective lines. The calculated intensity indicated by open histograms is in good agreement with the observed intensity shown by closed histograms in each sample. It is, therefore, reasonable to conclude that the trans and gauche conformations and the intramolecular hydrogen bonds are statistically formed in the frozen A-PVA solutions. The f_t and f_a values obtained in this analysis are also shown in Figure 5. The f_t and f_a values for the frozen DMSO-d_6 solution are significantly larger than those for the frozen aqueous solution. These results indicate that, in the frozen DMSO-d_6 solution, PVA chains are almost locally extended and most of successive possible OH groups, which are in the *m* sequences in this solvent

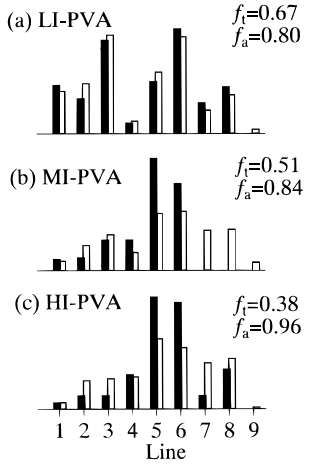

Figure 6. Histograms for observed and calculated relative intensities for the nine constituent lines in the frozen DMSO-d_6 solutions for PVA samples with different isotacticities. The closed and open histograms indicate observed and calculated intensities, respectively.

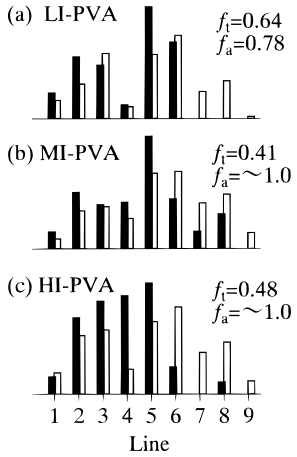

Figure 7. Histograms for observed and calculated relative intensities for the nine constituent lines in the frozen aqueous solutions for PVA samples with different isotacticities. The closed and open histograms indicate observed and calculated intensities, respectively.

because of the high f_t value, are able to form intramolecular hydrogen bonds. In the frozen aqueous solution, in contrast, the mole fraction of C−C bonds adopting the gauche conformation is considerably increased along the PVA chains and the probability for the formation of the intramolecular hydrogen bond is greatly reduced. These differences in conformation and intramolecular hydrogen bonding may be the differences in the physicochemical interaction between PVA chains and the solvents; the solvation with DMSO-d_6 will induce the local extension of PVA chains and preferential formation of intramolecular hydrogen bonds for atactic PVA. The interaction between DMSO molecules and OH groups seems not to be strongly associated with the solvation in this system. The detailed mechanism of the solvation in the PVA system will be clarified by using the molecular dynamic treatment in near future. It should be additionally noted that the difference in solvation also reflects on the difference in the probability for the formation of the intramolecular hydrogen bond in the crystalline state; it has already been found that more intramolecular hydrogen bonds are preferably formed in A-PVA films prepared from the DMSO solution than in those prepared from the aqueous solution.[11]

As is described above, the CH resonance lines of frozen A-PVA solutions are found to be well reproduced by the Bernoulli statistical calculations assuming the random distribution of trans and gauche conformations and the statistical formation of intramolecular hydrogen bonds. This indicates that the frozen-state CP/MAS ^{13}C NMR method is very powerful for the characterization of the conformation and the intramolecular hydrogen bond in the frozen PVA solutions. The same analysis for the noncrystalline components of different PVA films and fibers will be published somewhere in the near future.

Similar line shape analyses of CH resonance lines have well been conducted for the frozen DMSO-d_6 and aqueous solutions of different isotactic PVA samples. Figures 6 and 7 show the observed intensities obtained by the line shape analyses and the calculated intensities that were tried to fit with the observed ones by the least-squares method. In the frozen LI-PVA/DMSO-d_6 solution, the calculated intensity is still in good accord with the observed intensity, as seen in Figure 6a. In contrast, we cannot obtain any good accordance between observed and calculated intensities any more for PVA samples with higher isotacticies, as shown in Figure 6b,c. Furthermore, in the case of the frozen aqueous solution, no good accordance can be obtained even for the PVA sample (LI-PVA) with lower isotacticity, as is seen in Figure 7. Such discordances suggest that the treatment based on Bernoullian statistics described above may be inappropriate for PVA samples with higher isotacticities. There are two possible ways to interpret the discordances; other types of statistics such as Markov statistics should be applied to these samples or there may be the preferential formation of specific conformational structures. As for Markov statistics, there is no effect of this statistics on the determination of the mole fractions of the triad tacticities appearing in eq 6, because these fractions were directly determined by solution-state ^{13}C NMR spectroscopy, as described in the Experimental Section. We also tried to interpret the relative intensities shown in Figures 6 and 7 by using first-order Markov statistics for the distribution of the trans and gauche conformations along the PVA chains. However, we could not obtain much improved results.

In contrast, it may be highly plausible to assume that some specific structure is partly formed for PVA samples with higher isotacticities. For example, lines 5 and 6, which are the two prominent lines in Figure 6b,c, may be ascribed to the CH carbons in sequences with *tg* and $ttg^+g^-tg^-$ conformations, respectively. These conformations give helical structures, as shown in Figure 8. Since helical structures are dominantly produced in the crystalline state for vinyl polymers with high isotacticities, it will be reasonable to presume that a certain helical structure is partly formed for isotactic PVA samples in the frozen solution state. In this case solvated OH groups will induce such a helical structure through larger steric hindrance with each other compared to the case for free OH groups.

Analysis for the CH_2 Resonance Line. A similar analysis has also been conducted for the CH_2 resonance line, considering only the γ-gauche effect due to the CH_2 carbon. When the downfield shift of this effect is assumed to be −5.2 ppm (γ_{C-C} = −5.2 ppm[18]), three lines 1−3 with different chemical shifts are possibly recognized; −0 ppm for *t*@·@*t*, −5.2 ppm for *t*@·@*g*, and

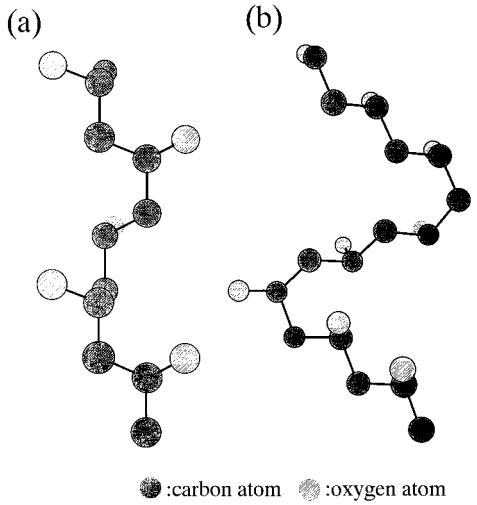

Figure 8. Schematic models of specific chain conformations possibly produced in the frozen DMSO-d_6 solutions of PVA with higher isotacticities: (a) *tg* conformation for line 5; (b) $ttttg^+g^-$ conformation for line 6.

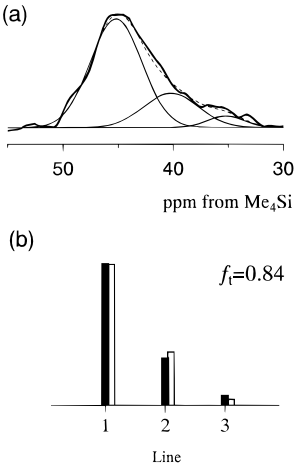

Figure 9. (a) Line shape analysis for the CH_2 resonance line of the frozen A-PVA aqueous solution. The broken line indicates the composite curve of the constituent lines shown by thin solid lines. (b) Histograms for the observed and calculated relative intensities for the three constituent lines in the frozen A-PVA aqueous solution. The closed and open histograms indicate observed and calculated intensities, respectively.

−10.4 ppm for *g*@•@*g*. The line shape analysis has been performed only for the frozen PVA aqueous solution, because the CH_2 resonance line of PVA is seriously superposed on the contribution from the residual CH_3 carbon of DMSO in the frozen PVA/DMSO-d_6 solution, as is seen in Figure 1. Figure 9 shows the result of the line shape analysis for the CH_2 resonance line of the frozen A-PVA aqueous solution and the histograms for the observed and calculated intensities. The observed CH_2 resonance line is found to be well resolved into three constituent lines described above. The observed intensities thus obtained for these lines are also well interpreted in terms of the statistical treatment, as shown in Figure 9b. The f_t value obtained by this analysis, which is also given in Figure 9b, is in good agreement with the value obtained for the CH resonance line (cf. Figure 5b). This indicates that the conformation and hydrogen bonding are statistically formed along the whole atactic PVA chains in the frozen aqueous solution.

Conclusion

Frozen-solution-state CP/MAS ^{13}C NMR analyses have been applied to the DMSO-d_6 and aqueous solutions of PVA samples with different tacticities and the following conclusions have been obtained:

The CH resonance lines of the frozen PVA solutions, which are greatly different in line splitting from those of PVA films, significantly depend on the solvents and tacticities.

The evaluation of upfield shifts due to the γ-gauche effect and the downfield shifts induced by the intramolecular hydrogen bonds indicates that there will appear nine lines with different chemical shifts. Using these lines, the CH resonance lines observed for different frozen PVA solutions are successfully resolved into the constituent lines by the line shape analyses.

The equations for the relative intensities of the nine constituent lines have been derived as functions of the probability f_a for the statistical formation of the intramolecular hydrogen bond and the probability f_t of the random distribution of the trans conformation along the PVA chains.

Observed and calculated intensities are in good accord with each other for the frozen A-PVA solutions, suggesting the statistical formation of the intramolecular hydrogen bonds and the random distribution of trans and gauche conformations in these systems. f_t and f_a values can be also determined through this analysis.

In contrast, the observed intensities for the frozen solutions of PVA samples with higher isotacticities are in disagreement with the calculated intensities obtained by the statistical treatment, suggesting that some specific conformations are preferably formed for isotactic PVA samples.

Appendix

To obtain the probability f_i^{mm} shown in Table 3, the following calculations are conducted by considering all possible conformations and intramolecular hydrogen bonds. At first, we consider the upfield shifts of the CH resonance line by the γ-gauche effect in the case of no formation of the intramolecular hydrogen bonding. The probabilities for certain conformations in the two successive C−C bonds at the left side of the central CH carbon in the *mm* sequence CH(OH)−CH_2−CH(OH)−CH_2−CH(OH) are given by the following probability matrix $\boldsymbol{U}_{lN}$:

$$\boldsymbol{U}_{lN} = \begin{array}{c} \\ (t) \\ (g^+) \\ (g^-) \end{array} \begin{array}{c} \begin{array}{ccc} (t) & (g^+) & (g^-) \end{array} \\ \begin{bmatrix} (1-f_a)f_t^2 & f_t f_{g^+} & f_t f_{g^-} \\ f_{g^+} f_t & f_{g^+} f_{g^+} & f_{g^+} f_{g^-} \\ f_{g^-} f_t & (1-f_a) f_{g^-} f_{g^+} & f_{g^-}{}^2 \end{bmatrix} \end{array} \qquad \text{(A-1)}$$

Here, the conformations for elements u_{ij} are defined for the two successive C−C bonds in the order from the left side in the *mm* sequence described above. Each element of this matrix is represented by using f_t, f_{g^+}, and f_{g^-} ($f_t + f_{g^+} + f_{g^-} = 1$). The probability f_a that the intramolecular hydrogen bond is formed for appropriate neighboring OH groups is also necessary for describing the matrix because the intramolecular hydrogen bonding is allowed to form in the *tt* and g^-g^+ conformations. Another matrix $\boldsymbol{U}_{rN}$, which has the same elements as those for $\boldsymbol{U}_{lN}$, should also be defined for conformations in the two successive C−C bonds at the right side in the *mm* sequence.

The total probability matrix $\boldsymbol{U}_{NN}$ for all conformations of the four successive C−C bonds in the *mm* sequence associated with no intramolecular hydrogen bonding is expressed as the direct product[21] of $\boldsymbol{U}_{lN}$ and $\boldsymbol{U}_{rN}$:

$$\boldsymbol{U}_{NN} = \boldsymbol{U}_{lN} \otimes \boldsymbol{U}_{rN} \tag{A-2}$$

The calculation of eq A-2 gives the 9 × 9 matrix, and the elements indicate the probabilities of all possible conformations in the *mm* sequence.

The upfield shifts due to the γ-gauche effect induced for the respective conformations in the *mm* sequence will be also expressed as shift matrix $\Delta\delta_{NN}$. This matrix is the direct sum of the matrixes δ_{lN} and δ_{rN}, which are the contributions at the left and right sides for the central CH carbon in question, respectively:

$$\Delta\delta_{NN} = \delta_{lN} \oplus \delta_{rN} \tag{A-3}$$

with

$$\delta_{lN} = \begin{array}{c} \\ (t) \\ (g^+) \\ (g^-) \end{array} \begin{array}{c} \begin{array}{ccc} (t) & (g^+) & (g^-) \end{array} \\ \begin{bmatrix} -7.2 & -7.2 & -7.2 \\ -5.9 & -5.9 & -5.9 \\ -13.1 & -13.1 & -13.1 \end{bmatrix} \end{array}$$

$$\delta_{rN} = \begin{array}{c} \\ (t) \\ (g^+) \\ (g^-) \end{array} \begin{array}{c} \begin{array}{ccc} (t) & (g^+) & (g^-) \end{array} \\ \begin{bmatrix} -7.2 & -13.1 & -5.9 \\ -7.2 & -13.1 & -5.9 \\ -7.2 & -13.1 & -5.9 \end{bmatrix} \end{array} \tag{A-4}$$

Here, the direct sum is defined in the analogy of the direct product[21] as follows:

$$\boldsymbol{X} \otimes \boldsymbol{Y} = \begin{bmatrix} x_{11} & x_{12} \\ x_{21} & x_{22} \end{bmatrix} \oplus \begin{bmatrix} y_{11} & y_{12} \\ y_{21} & y_{22} \end{bmatrix} =$$

$$\begin{bmatrix} \begin{pmatrix} x_{11}+y_{11} & x_{11}+y_{12} \\ x_{11}+y_{21} & x_{11}+y_{22} \end{pmatrix} & \begin{pmatrix} x_{12}+y_{11} & x_{12}+y_{12} \\ x_{12}+y_{21} & x_{12}+y_{22} \end{pmatrix} \\ \begin{pmatrix} x_{21}+y_{11} & x_{21}+y_{12} \\ x_{21}+y_{21} & x_{21}+y_{22} \end{pmatrix} & \begin{pmatrix} x_{22}+y_{11} & x_{22}+y_{12} \\ x_{22}+y_{21} & x_{22}+y_{22} \end{pmatrix} \end{bmatrix} \tag{A-5}$$

As a result, six states with different chemical shifts are found to exist according to the differences in the γ-gauche effect.

In the case of PVA, we should further consider the formation of the intramolecular hydrogen bonding, which induces the appreciable downfield shift for the CH resonance line. Since the intramolecular hydrogen bonding in the *mm* sequence is allowed to form in *tt* and g^-g^+ conformations, the probability matrix $\boldsymbol{U}_{lA}$ for the conformations associated with the intramolecular hydrogen bond between the two OH groups at the left side in the *mm* sequence is given by

$$\boldsymbol{U}_{1A} = \begin{array}{c} \\ (t) \\ (g^+) \\ (g^+) \end{array} \begin{array}{c} \begin{array}{ccc} (t) & (g^+) & (g^-) \end{array} \\ \begin{bmatrix} f_a f_t^2 & 0 & 0 \\ 0 & 0 & 0 \\ 0 & f_a f_{g^+} f_{g^-} & 0 \end{bmatrix} \end{array} \tag{A-6}$$

The same equation as eq A-6 is given for the probability matrix $\boldsymbol{U}_{rA}$ that describes the probabilities for the conformations associated with the formation of the intramolecular hydrogen bond for the two OH groups at the right side in the *mm* sequence. As a result of the combination of those four matrixes $\boldsymbol{U}_{lA}$, $\boldsymbol{U}_{rA}$, $\boldsymbol{U}_{lN}$, and $\boldsymbol{U}_{rN}$, three other total probability matrixes associated with the intramolecular hydrogen bonding are given by

$$\begin{aligned} \boldsymbol{U}_{AA} &= \boldsymbol{U}_{lA} \otimes \boldsymbol{U}_{rA} \\ \boldsymbol{U}_{AN} &= \boldsymbol{U}_{lA} \otimes \boldsymbol{U}_{rN} \\ \boldsymbol{U}_{NA} &= \boldsymbol{U}_{lN} \otimes \boldsymbol{U}_{rA} \end{aligned} \tag{A-7}$$

Three chemical shift matrixes, which correspond to those three total probability matrixes, are also given for the corresponding total probability matrixes by evaluating both of the γ-gauche effect and the intramolecular hydrogen bonding:

$$\begin{aligned} \Delta\delta_{AA} &= \delta_{lA} \oplus \delta_{rA} \\ \Delta\delta_{AN} &= \delta_{lA} \oplus \delta_{rN} \\ \Delta\delta_{NA} &= \delta_{lN} \oplus \delta_{rA} \end{aligned} \tag{A-8}$$

with

$$\delta_{lA} = \begin{array}{c} \\ (t) \\ (g^+) \\ (g^-) \end{array} \begin{array}{c} \begin{array}{ccc} (t) & (g^+) & (g^-) \end{array} \\ \begin{bmatrix} -1.3 & 0 & 0 \\ 0 & 0 & 0 \\ 0 & -5.9 & 0 \end{bmatrix} \end{array}$$

$$\delta_{rA} = \begin{array}{c} \\ (t) \\ (g^+) \\ (g^-) \end{array} \begin{array}{c} \begin{array}{ccc} (t) & (g^+) & (g^-) \end{array} \\ \begin{bmatrix} -1.3 & 0 & 0 \\ 0 & 0 & 0 \\ 0 & -5.9 & 0 \end{bmatrix} \end{array} \tag{A-9}$$

As a result, the probabilities f_i^{mm} as shown in Table 3 are obtained by the calculation of eqs A-2 and A-7 and their chemical shifts are also obtained from eqs A-4 and A-8. Similar calculations can also be performed for probabilities f_i^{mr} and f_i^{rr} in the *mr* and *rr* sequences, respectively.

References and Notes

(1) Sakurada, I. *Polyvinyl Alcohol Fibers*; Marcel Dekker: New York, 1985.
(2) Finch, C. A., Ed. *Polyvinyl Alcohol -Developments*; John Wiley & Sons: Chichester, U.K., 1992.
(3) Terao, T.; Maeda, S.; Saika, A. *Macromolecules* **1983**, *16*, 1535.
(4) Horii, F.; Hu, S.; Ito, T.; Kitamaru, R.; Matsuzawa, S.; Yamaura, K. *Polymer* **1992**, *33*, 229.
(5) Hu, S.; Tsuji, M.; Horii, F. *Polymer* **1994**, *35*, 9516.
(6) Ketel, H.; Haan, J.; Aerdts, A.; Velden, G. *Polymer* **1990**, *31*, 1419.
(7) Imashiro, F.; Obara, S. *Macromolecules* **1995**, *28*, 2840.
(8) Hu, S.; Horii, F.; Odani, H. *Bull. Inst. Chem. Res., Kyoto Univ.* **1991**, *69*, 165.
(9) Hu, S. Ph.D. Dissertation, Kyoto University, 1991.
(10) Hu, S.; Horii, F.; Odani, H.; Narukawa, H.; Akiyama, A.; Kajitani, K. *Kobunshi Ronbunshu* **1992**, *49*, 361.
(11) Masuda, K.; Hu, S.; Kaji, H.; Horii, F. *Polym. Prepr., Jpn.* **1996**, *45*, 3260; in preparation for publication.
(12) Bunn, C. W. *Nature* **1948**, *161*, 929.
(13) Sakurada, I.; Futino, K.; Okada. *Bull. Inst. Chem. Res., Kyoto Univ.* **1950**, *23*, 78.
(14) Horii, F.; Masuda, K.; Kaji, H. *Macromolecules* **1997**, *30*, 2519.
(15) Ohgi, H.; Sato, T. *Macromolecules* **1993**, *26*, 559.
(16) Horii, F.; Hirai, A.; Kitamaru, R.; Sakurada, I. *Cellulose Chem. Technol.* **1985**, *19*, 513.
(17) Torchia, D. A. *J. Magn. Reson.* **1981**, *44*, 117.
(18) Tonelli, A. E. *NMR Spectroscopy and Polymer Microstructure: The Conformational Connection*; VCH: New York, 1989.

(19) Born, R.; Spiess, H. W. *Ab Initio Calculations of Conformational Effects on ^{13}C NMR Spectra of Amorphous Polymers;* Springer: Berlin, 1997.

(20) Imashiro, F.; Maeda, S.; Takegoshi, K.; Terao, T.; Saika, A. *Chem. Phys. Lett.* **1983**, *99*, 189.

(21) Flory, P. J. *Statistical Mechanics of Chain Molecules*; Interscience Publishers: New York, London, Sydney, Toronto, 1969.

MA9801265